# Coexisting Modes and Bifurcation Structure in a Pair of Coupled Detuned Third Order Oscillators

B Shayak[1], Aditya Bhaskar[1], Alan T. Zehnder[1], and Richard H. Rand[*1, 2]

[1]Theoretical and Applied Mechanics, Sibley School of Mechanical and Aerospace Engineering, Cornell University, Ithaca, New York, USA
[2]Department of Mathematics, Cornell University

February 13, 2020

**Abstract**

The bifurcation structure of a system of two non-linear coupled oscillators is considered here. This system is motivated by coupled micro-oscillators proposed for microelectromechanical systems (MEMS) applications. The model starts from previous work in which the authors considered the bifurcation structure in a pair of *identical* coupled, oscillators, each of which is modelled by a third-order nonlinear system. In the present paper, the case is considered where the two oscillators are non-identical i.e. *detuned* from each other. The series of bifurcations obtained is described in detail. It is seen that the symmetry of the bifurcation structure present in the identical oscillators is lost in the detuned oscillators. A very surprising homoclinic bifurcation is seen in one region of the parameter space, and this is examined in more detail through consideration of a simplified system.

## Keywords

synchronization, micro-oscillators, two-variable expansion, numerical analysis, Melnikov method, numerical continuation

## 1 Introduction

This work is a direct follow-up to research done by the authors in a recent work [1], which in turn draws upon their past study [2]. This series of works is motivated by the application of micron-scale resonators and oscillators used in microelectromechanical

[*]Corresponding author, rhr2@cornell.edu

systems (MEMS). One of the simplest structures, a cantilevered beam has found many applications. An early use was as micromechanical switches which exhibited much higher switching speeds compared to the then-conventional reed relay switch circuits [3]. Ma et. al. [4] have proposed a device where microcantilevers measure the flow rate and flow direction of a gas. An application of microcantilever as a resonator has been considered by Pratihar [5]. More recently, MEMS cantilevers have found applications in biological arena – for example, Dhakane and Patil [6] have proposed a device for tuberculosis detection in patients. A novel technology for improving the sensitivity of microcantilever in biological applications has been described by Parsediya et. al. [7] who propose a variable-width design which achieves greater deflection of the tip for the same molecular pressure. Ansari and Cho [8] propose an optimized miocrocantilever sensor for surface stress studies, with applications to the study of physical, chemical and biological phenomena.

Coupled micro-oscillators have attracted considerable attention in the past. For example, as far back as 1999, Smith et. al. [9] observed intermittent chaos in a pair of pendula coupled by a mechanism which produced a torque proportional to the difference in their angular velocities. More recently, Yolong and Woafo [10] have considered a pair of micro-beam oscillators with electrostatic coupling, and observed chaos in this system. An even more detailed analysis of the chaotic regime in MEMS oscillators has been done by Amorim et. al. [11]. Whereas a majority of works, including the present work, feature linear coupling, nonlinear coupling has also been investigated in literature, for example by Romeo and his co-authors [12, 13] and by Shoshani et. al. [14].

In Refs. [1, 2, 15], it is seen that the micro-resonator illuminated by a laser satisfies a third order nonlinear differential equation. The displacement of the beam is governed by a second order equation while its temperature contributes an additional degree of freedom which couples to the mechanical dynamics. Such third order dynamical systems are quite rare compared to second order systems but are not absolutely unheard of. For example, Leadenham and Erturk [16, 17] have found such an equation in a problem where a piezoelectric material converts vibrational energy to electrical energy – the vibrations are governed by a second order equation while the electrical dynamics contribute an additional order. A similar model has been proposed by Garg and Dwivedi [18]. Kuznetsov et al. have designed a third order oscillator [19, 20] to demonstrate a quasiperiodic attractor. It is also noteworthy that the dynamic model of a current source-fed induction motor or a voltage source-fed permanent magnet synchronous motor is also third order nonlinear, while that of a voltage source-fed induction motor is fifth order nonlinear [21, 22, 23]. The general theory of stability of third order nonlinear systems can be found for example in the treatment by Tunc and Atez [24].

In Ref. [1], the dynamics of two coupled, identical micro-oscillators [2] was studied. In that work the model for a single oscillator takes the form

$$\ddot{z} + z = T \tag{1a}$$

$$\dot{T} + T = z^2 - pz \tag{1b}$$

where $z$ denotes the non-dimensional displacement of the beam and $T$ denotes its di-

mensionless temperature. The above model is a simplification of the system presented in refs. [2, 15]. This system exhibits limit cycle oscillations for $p > 0$, analogous to the behavior seen in MEMS devices transduced by laser interference [15].

The case of two linearly coupled *identical* oscillators of the form given in equation (1) was analyzed in detail in prior work [1]. It was found that at higher coupling strengths, the in-phase (IP) and out-of-phase (OP) modes were both stable. As the coupling strength was decreased, a complicated sequence of bifurcations led to loss of stability of the IP mode. The most striking feature of these bifurcations was the symmetry of the system. The method of two variable expansion was used on the system and the slow flow (sometimes known as amplitude equations or averaged equations) was obtained in terms of three variables $r_1$, $r_2$ and $\varphi$, denoting respectively the amplitudes of the two oscillators and the phase difference between them. This flow was found to be symmetric under the transformation $r_1 \to r_2$, $r_2 \to -r_1$ and $\varphi \to -\varphi$.

In contrast to the work just described, the current paper treats the case where the two oscillators are non-identical i.e. their natural frequencies are detuned from each other. In summary, one finds here a richer bifurcation sequence than in Ref. [1] on account of the detuning which breaks the symmetry mentioned in the above paragraph. The most important new feature is an unfolding of the single homoclinic bifurcation of the symmetric system into three different homoclinic bifurcations. This will be seen in detail presently.

## 2 Detuned model and slow flow

The governing equation for two coupled detuned oscillators is

$$\ddot{z}_1 + z_1 = T_1 + \alpha\,(z_2 - z_1) \tag{2a}$$

$$\dot{T}_1 + T_1 = z_1^2 - p z_1 \tag{2b}$$

$$\ddot{z}_2 + (1+k_1)^2 z_2 = T_2 + \alpha\,(z_1 - z_2) \tag{2c}$$

$$\dot{T}_2 + T_2 = z_2^2 - p z_2 \tag{2d}$$

where $k_1$ is the detuning parameter (difference in natural frequency between the two oscillators) and $\alpha$ the strength of the coupling between the two oscillators. The parameter $p$, which represents a static displacement of the MEMS oscillator relative to an experimental baseline, is the driver of the limit cycles. One finds from a linear stability analysis on (2) that the fixed point at the origin is stable for $p < 0$ and unstable for $p > 0$. At $p = 0$ the origin undergoes a Hopf bifurcation, which gives rise to the limit cycle. For the entire work, $p$ will be set to the fixed value 0.1 and its variation will not be considered further. This is the same as what has been done in Ref. [1].

The method of two-variable expansion [27] is used to obtain a slow flow. We start by scaling (2) in the following manner:

$$\ddot{z}_1 + z_1 = \varepsilon T_1 + \varepsilon^2 \alpha\,(z_2 - z_1) \tag{3a}$$

$$\dot{T}_1 + T_1 = z_1^2 - \varepsilon p z_1 \tag{3b}$$

$$\ddot{z}_2 + \left(1 + \varepsilon^2 k_1\right)^2 z_2 = \varepsilon T_2 + \varepsilon^2 \alpha \left(z_1 - z_2\right) \tag{3c}$$

$$\dot{T}_2 + T_2 = z_2^2 - \varepsilon p z_2 \tag{3d}$$

where $\varepsilon$ is a small parameter. We define three time-scales – regular time $\xi$, slow time $\eta$ and super-slow time $\zeta$. We expand the variables as $z_1 = z_{10} + \varepsilon z_{11} + \varepsilon^2 z_{12}$, $T_1 = T_{10} + \varepsilon T_{11} + \varepsilon^2 T_{12}$ and so on. Using a computer algebra system, we solve first the differential equations obtained by considering terms independent of $\varepsilon$. These are linear and easy to solve. Then, we substitute these solutions into the equations obtained by collecting terms of order $\varepsilon$. These solutions have resonance terms, which must be removed to obtain the slow flow. A trivial slow flow is obtained at $O(\varepsilon)$, necessitating the progression to $O(\varepsilon^2)$. At this stage, the following equations in the super-slow time, $\zeta$ are obtained, where $z_1 = A(\zeta)\cos\xi + B(\zeta)\sin\xi$ and $z_2 = C(\zeta)\cos\xi + D(\zeta)\sin\xi$,

$$\frac{\mathrm{d}A}{\mathrm{d}\zeta} = \frac{30p\left(A+B\right) + 60\alpha\left(B-D\right) - \left(27A+31B\right)\left(A^2+B^2\right)}{120} \tag{4a}$$

$$\frac{\mathrm{d}B}{\mathrm{d}\zeta} = \frac{30p\left(B-A\right) + 60\alpha\left(C-A\right) + \left(31A-27B\right)\left(A^2+B^2\right)}{120} \tag{4b}$$

$$\frac{\mathrm{d}C}{\mathrm{d}\zeta} = \frac{30p\left(C+D\right) + 60\alpha\left(D-B\right) - \left(27C+31D\right)\left(C^2+D^2\right) + 60k_1 D}{120} \tag{4c}$$

$$\frac{\mathrm{d}D}{\mathrm{d}\zeta} = \frac{30p\left(D-C\right) + 60\alpha\left(A-C\right) + \left(31C-27D\right)\left(C^2+D^2\right) - 60k_1 C}{120} \tag{4d}$$

It is noted that since the $T$-equations have exponentially decaying solutions at the largest order, they are not characterized by independent dynamical variables. Rather, the temperatures exhibit limit cycle oscillations which are completely locked to the $z$-oscillations [1] and occur at twice the frequency. Specifically, for a single oscillator, the following has been found in [1]:

$$T = A^2\left(\frac{1}{2} + \frac{1}{5}\sin 2\omega t + \frac{1}{10}\cos 2\omega t\right) \tag{5}$$

where $A$ denotes the amplitude of the $z$ oscillation. Hence the dynamics of $T$ will be neglected in the subsequent discussion.

To facilitate the analysis, the variables in (4) are transformed to polar coordinates $A = r_1\cos\theta_1$, $B = r_1\sin\theta_1$, $C = r_2\cos\theta_2$ and $D = r_2\sin\theta_2$. Only the relative phase $\varphi = \theta_2 - \theta_1$ has any significance in the dynamics. The evolution equations for $r_1$, $r_2$ and $\varphi$ are,

$$\frac{\mathrm{d}r_1}{\mathrm{d}\zeta} = \frac{pr_1}{4} - \frac{9r_1^3}{40} - \frac{\alpha}{2}r_2\sin\varphi \tag{6a}$$

$$\frac{\mathrm{d}r_2}{\mathrm{d}\zeta} = \frac{pr_2}{4} - \frac{9r_2^3}{40} + \frac{\alpha}{2} r_1 \sin\varphi \tag{6b}$$

$$\frac{\mathrm{d}\varphi}{\mathrm{d}\zeta} = \frac{31}{120}\left(r_2^2 - r_1^2\right) + \frac{\alpha\cos\varphi}{2}\left(\frac{r_1}{r_2} - \frac{r_2}{r_1}\right) - \frac{k_1}{2} \tag{6c}$$

In the limit of $k_1 = 0$ this agrees with the results of Reference [1].

In what follows we shall analyse (6) to determine various dynamical features such as equilibria, their stabilities, limit cycles including those born in Hopf bifurcations, etc. The presence of such features in the slow flow (6) has implications about the corresponding behaviour in the physical model (2). For example, a stable equilibrium point in the slow flow corresponds to a periodic motion (a stable limit cycle) in the original system. A limit cycle in (6) corresponds to a quasiperiodic motion in (2).

# 3 Structure of the bifurcations

Before describing the details an overview of the bifurcation structure is first described. A variety of semi-analytical and numerical procedures were used to understand the bifurcation sequence of the oscillators. The overall bifurcation diagram obtained in the $k_1$-$\alpha$ plane is shown in Fig. 1. Corresponding to each transition, a curve has been indicated. The schematic phase portraits of the system, projected onto the $r_1$-$r_2$ plane in the labelled regions, are as shown in Fig. 2.

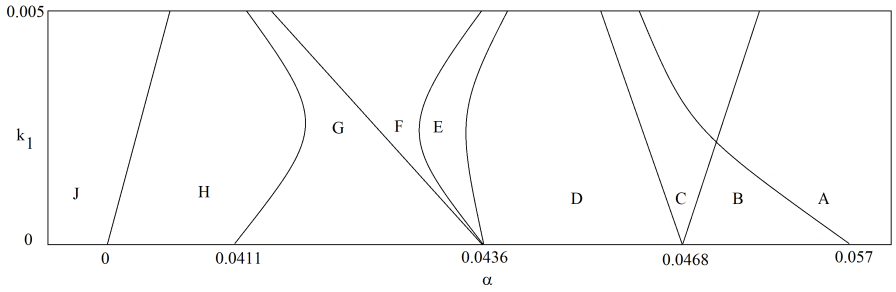


Figure 1: Bifurcation curves of the slow flow (5) in the $k_1$-$\alpha$ plane. Note that $k_1$ is the detuning while $\alpha$ is the coupling. The line separating regions A and B corresponds to saddle node bifurcations. The lines separating B,C and C,D corespond to Hopf bifurcations. D-E, E-F and F-G are homoclinic bifurcations, G-H is a saddle node bifurcation of limit cycles while H-J is again a saddle node. Details will be explained in the subsequent text.

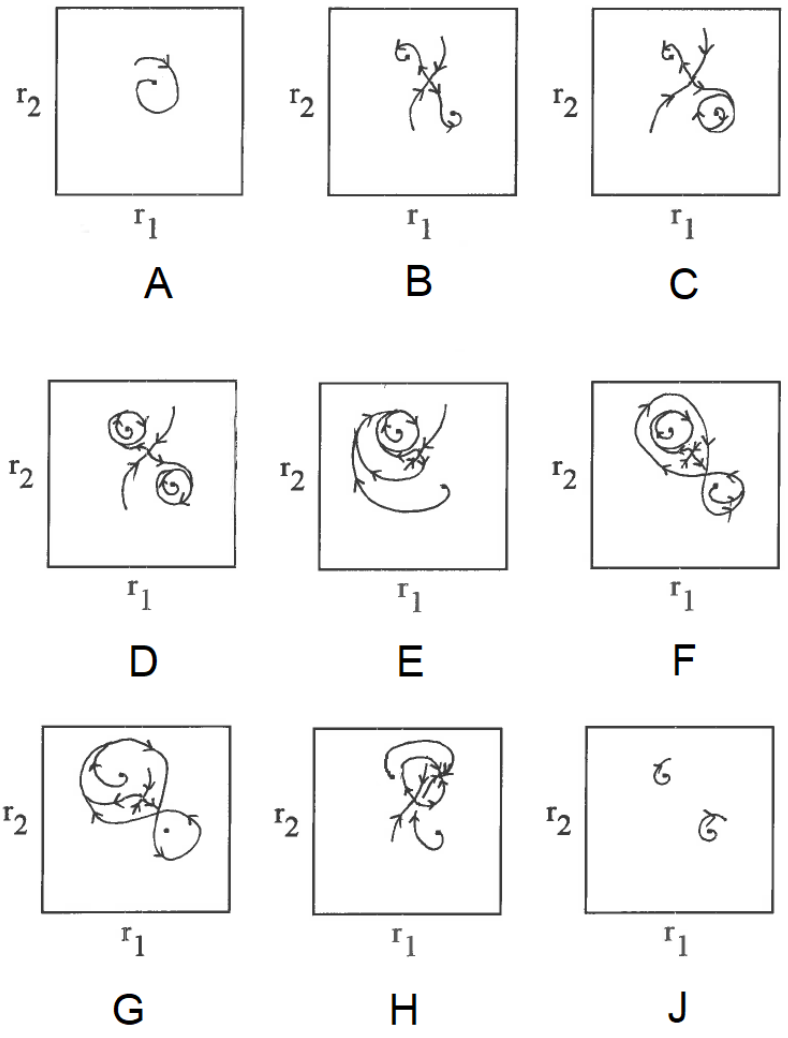


Figure 2: Trajectories in the $r_1$-$r_2$ plane in each of the labelled regions shown in Fig. 1. These represent two-dimensional projections of three-dimensional trajectories, hence certain unintuitive features, such as intersecting trajectories, are seen in this case. Most of the diagrams can be explained on the basis of the subsequent text. In H, all trajectories go to the OP mode which is stable in regions A to G also but is not shown in any of the previous diagrams for clarity.

The derivation of this diagram shall now be described. For $\alpha$ sufficiently large, only the in-phase (IP) mode is stable. It is also noted that an exact IP mode is no longer a solution of the detuned equations (3) and (5) – rather, there exists an IP-like solution

which features $r_1$ and $r_2$ very close to each other and $\varphi$ very small. Nevertheless, we shall continue to refer to this solution as the IP mode, trading lexical accuracy for conciseness of expression. As $\alpha$ is decreased, a complex series of bifurcations occurs as shown in Fig. 1. The first few of these bifurcations (A, B, and C) were obtained by using AUTO Bifurcation Software [25] on the slowflow (6). This software performs numerical continuation and yields the saddle node and Hopf bifurcation transition lines. The first bifurcation obtained in Reference [1] (based on a symmetric model of two identical oscillators) was a pitchfork at $\alpha = 0.057$ which led to the stable IP mode turning unstable while a new pair of stable fixed points was born. In the present work, the symmetry of the previous study is broken by the detuning. The pitchfork is replaced by a saddle node where the two new fixed points are born. One of these becomes the new IP mode while the original IP mode deviates considerably and becomes the "mirror image" of the other point born in the saddle node. It turns out that an analytical formula can be found for the saddle node bifurcation curves - this process is described below. Due to length of expressions involved, computer algebra is used for this purpose. The software WXMaxima is employed; the script used is given in the Appendix.

One starts by hunting for the fixed points of the slow flow (5). To do this analytically, one obtains an expression for $\sin\varphi$ from (5a) and one for $\cos\varphi$ from (5c) and then uses $\sin^2\varphi + \cos^2\varphi = 1$. This yields a polynomial equation for $r_1$ and $r_2$. A second polynomial equation can be obtained in an analogous fashion by using this trigonometric identity between (5b) and (5c). Thereafter, the variable $r_2$ is eliminated between these two polynomials to obtain a single equation for $r_1$. This equation is of the 48th degree. Since a saddle node (or pitchfork) corresponds to a double root, one has the condition that the derivative of the above polynomial with respect to $r_1$ be also zero. Eliminating between these two conditions leads to a relation between $k_1$ and $\alpha$, this eliminant taking the form

$$P_{14}(\alpha, k_1) = 0 \tag{7}$$

where $P_{14}$ denotes a polynomial of the 14th degree, which is too lengthy to quote in full.

For $k_1 = 0$, $P_{14}(\alpha, 0)$ simplifies considerably and factorizes as

$$P_{14}(\alpha) = (\alpha - 31/540)P_{13}(\alpha) \tag{8}$$

where $P_{13}$ has only negative real and complex roots, which are physically meaningless. Thus, one obtains the critical value $\alpha = \alpha_{cr} = 31/540$ as the location of the pitchfork. This matches with what has been obtained in Reference [1]. One then substitutes $\alpha = \alpha_{cr} + \delta\alpha$ into $P_{14}$ and sets this equal to zero. For small values of $k_1$ and $\delta\alpha$, the largest term in this expression which is independent of $k_1$ is $\delta\alpha^3$ while the largest term independent of $\delta\alpha$ is $k_1^2$. To satisfy the equation, these two terms must balance each other, giving the power law relationship $k_1 \sim \delta\alpha^{3/2}$. The numerical coefficient happens to evaluate to $(1077/4155)^{1/3} = 0.6376$, thus implying that near the critical point,

$$\alpha_{cr} - \alpha = 0.6376 k_1^{2/3} \tag{9}$$

In Fig. 3, this curve is shown superposed on the curve of saddle node bifurcations obtained by AUTO. The agreement is good near $\alpha_{cr}$ and deteriorates as one moves away from it, as expected given the assumptions leading to this conclusion.

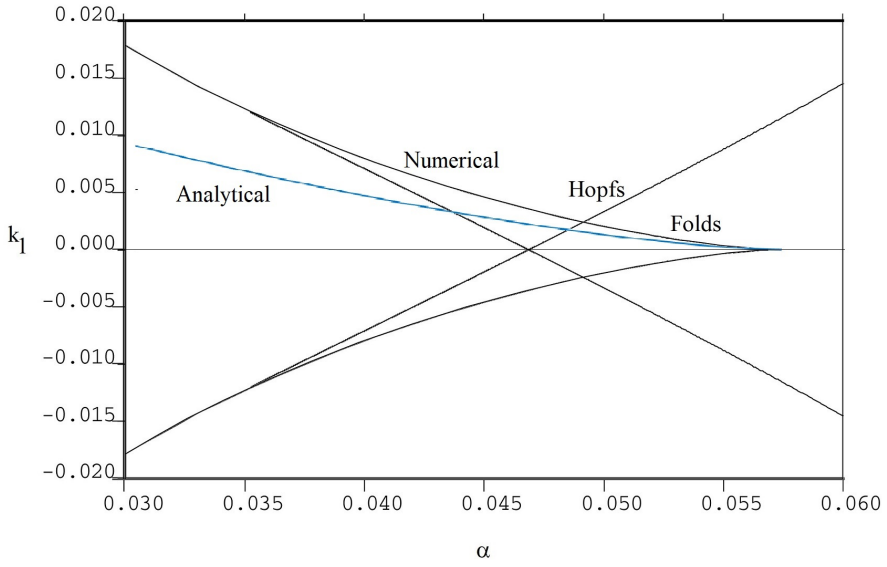


Figure 3: Black lines show the bifurcation diagram of (5) as plotted by AUTO. The lines marked as "fold" are where saddle-node bifurcations occur – in the upper half-plane, a pair of fixed points are born in a saddle node as one crosses the line from below. The lines marked "Hopf" show the same for Hopf – the fixed points born in the saddle-node bifurcation lose stability in a Hopf bifurcation as one crosses the line from the right. The diagram is symmetric with respect to the $\alpha$-axis. The blue line labelled "analytical" shows the curve $\alpha_{cr} - \alpha = 0.6376 k_1^{2/3}$, as described in the text.

In the identical oscillators, the next bifurcation upon decreasing $\alpha$ was a double-Hopf at $\alpha = 0.0468$. Both the stable fixed points created in the pitchfork lost stability in Hopf bifurcations. Here, the two Hopfs do not occur simultaneously but one after the other. Thus, at a detuning of, for example, $k_1 = 0.002$, the IP-like mode loses stability prior to the other stable fixed point which was created in the saddle node. In fact, the Hopf bifurcation actually occurs before the saddle node. At negative detuning on the other hand, the IP mode retains stability for a longer range than the other fixed point.

The subsequent bifurcation in the identical system was a homoclinic bifurcation at $\alpha = 0.0436$ in which the two limit cycles created in the Hopfs crashed into each other and formed one big limit cycle. In the presence of frequency-detuning, a very interesting behaviour takes place. The following sequence is found : (i) one of the two limit cycles born in the Hopf approaches the saddle, crashes into it and vanishes, (ii) the other limit cycle born in the Hopf approaches closer to the saddle without yet touching it, (iii) a connection takes place betwen a transient trajectory approaching this limit cycle and an unstable trajectory leaving the Hopf point, giving rise to a second stable

limit cycle, which has a figure of eight shape in the $r_1$-$r_2$ plane, (iv) the earlier limit cycle and the new figure-of-eight cycle coexist stably, (v) the smaller cycle impacts the saddle and vanishes, leaving only the figure-of-eight cycle. This phenomenon is illustrated through Figs. 4 to 6, in which the value $k_1 = 0.002$ is taken as a reference.

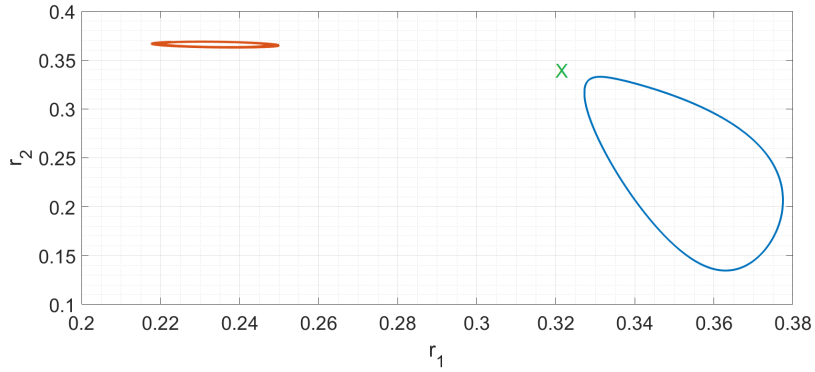


Figure 4: Region D of Figs. 1-2. The two limit cycles born in the Hopf bifurcations in the $r_1 - r_2$ plane at $\alpha = 0.0450$. Different initial conditions go to the two limit cycles - two non-specific values have been chosen for the figure. The saddle-like IP mode is also shown as a X.

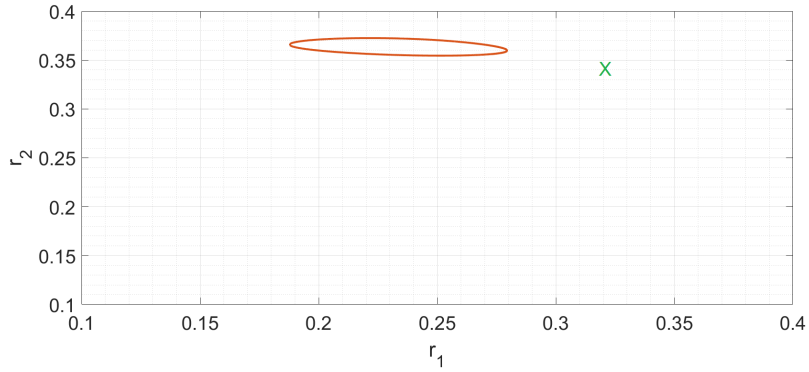


Figure 5: Region E. At $\alpha = 0.0440$, only one of the above two limit cycles exists.

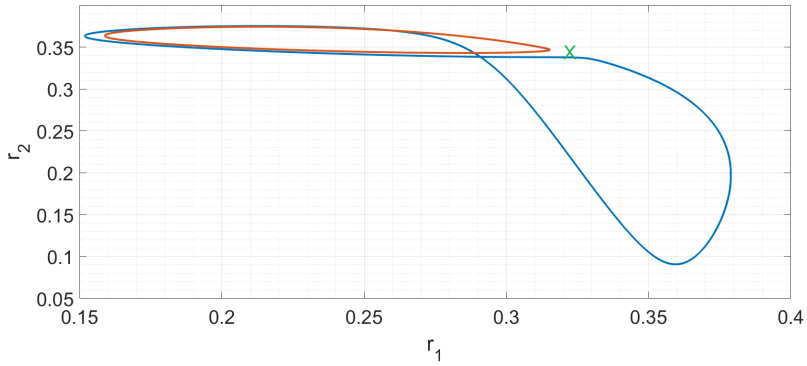


Figure 6: Region F. Coexistence of the limit cycle from Fig. 5 with a figure-of-eight limit cycle is seen at $\alpha = 0.0427$. Recall that the apparent self-intersection is the result of projection of a three-dimensional dynamics onto the $(r_1, r_2)$ plane. This rather surprising coexistence has been mentioned by Hubbard and West [26] in the context of a simpler system.

The next bifurcation is common to both the identical and detuned systems. The figure-of-eight limit cycle crashes into the separatrix which demarcates the out-of-phase motions from the in-phase ones, and is lost. Only the OP motion is stable from this point onwards.

The detuned system has a bifurcation at really small $\alpha$ which does not exist in the identical system. This is a transition from OP mode to drift. When the coupling is reduced to less than $\alpha = 0.001$, the two oscillators start evolving in time independently of each other. This is illustrated by the time trace of $\varphi(t)$ in Fig.7, showing that the phases diverge. By solving for the fixed points of the slow flow, it was found that a saddle-node bifurcation occurs at this point; as $\alpha$ is decreased through the critical value, the stable OP and unstable IP modes come together and disappear as shown in Fig. 8.

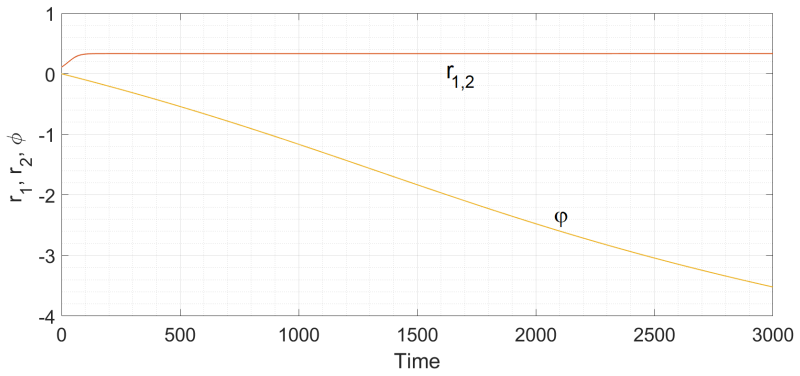


Figure 7: Region J. At $\alpha = 0.0003$, the time traces of $r_1$ and $r_2$ overlap with each going to a fixed value, while that of $\varphi$ shows continuous increase in time, indicating that the oscillators are drifting.

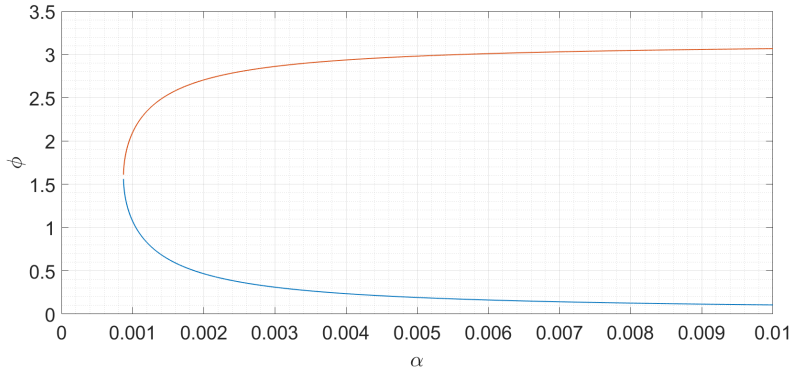


Figure 8: $\varphi$ vs. $\alpha$ for the IP and OP modes at fixed $k_1 = 0.002$. It can be seen that as $\alpha$ approaches about 0.0009 from above, $\varphi$ approaches $\pi/2$ for both modes which coalesce in a saddle-node bifurcation.

Primarily numerical methods were used to obtain the transition curves between the regions D to J. A detailed diagram of the regions D to H is shown in Fig. 9. To generate this Figure, at each point in the $(\alpha, k_1)$ parameter space, 21 initial conditions were taken at random from the intervals $r_1$, $r_2$ belonging to $[0, 0.5]$ and $\varphi$ belonging to $[0, \pi/6]$, and the steady state response of the system was determined.

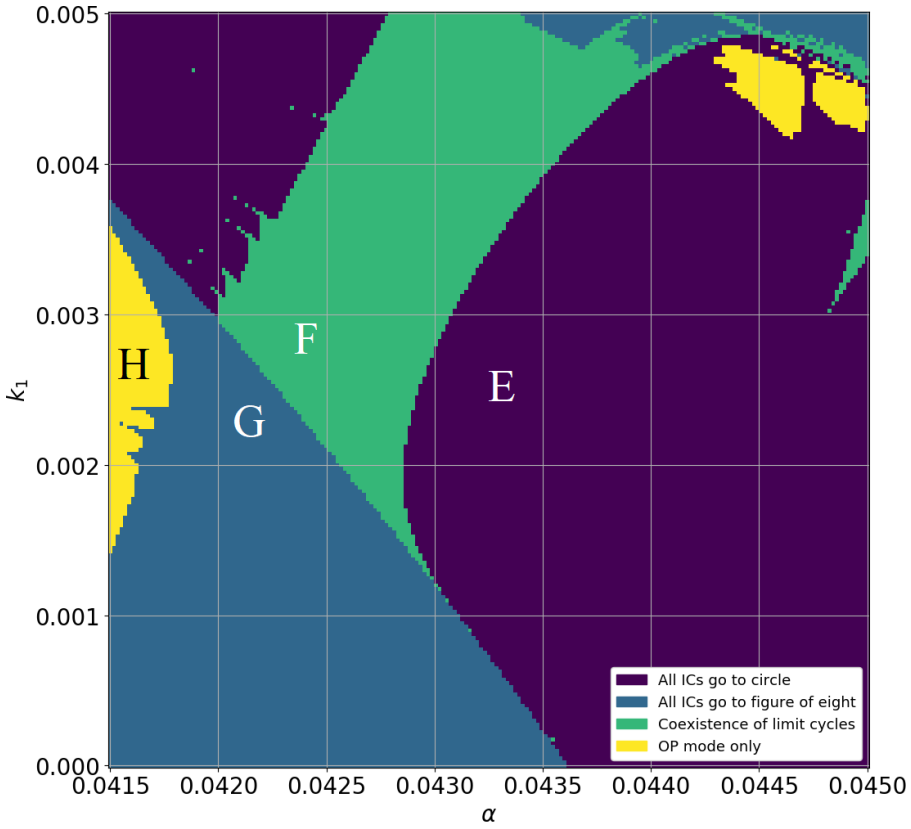


Figure 9: Simulation results for the slow flow (6). For each point in this diagram, 21 different initial conditions were chosen at random and the results of numerical integration with those initial conditions were noted. Since the OP mode is stable throughout, it is understood that some initial conditions will go to that mode. If ALL initial conditions go to OP, then the point in the parameter space has been marked as yellow. Else, if the only possibilities are OP mode and a circle-shaped (small) limit cycle in the $r_1$-$r_2$ plane, then the point has been marked as purple. Else, if the only possibilities are OP mode and figure-of-eight shaped limit cycle, then the point has been marked with blue. Finally, those regions where both circle and figure-of-eight limit cycles are stable have been shown in green. Homoclinic bifurcations occur as one transitions from the purple to the green and green to blue regions. The curves shown in Fig. 1 have been drawn on the basis of this diagram. The appearance of the irregular regions in the upper right as well as a purple region to the left of the green region for high $k_1$ is puzzling, and cannot be accounted for by the simplified model of the following Section.

To gain additional insight into the system dynamics, we investigate whether a similar bifurcation structure can be found in a simpler system as well. The analysis is described in the next Section.

# 4 Analysis of a simplified system

As a simpler form of the slowflow (6), the authors considered the second order system

$$\ddot{x} - x + x^3 - b\dot{x} + \dot{x}^3 + \beta x^2 = 0 \tag{10}$$

This system was constructed as a pedagogical model to illustrate the homoclinic bifurcations occurring in the original system. In this model, one needed the equation to exhibit two small limit cycles on either side of a saddle point plus one larger limit cycle (the figure-of-eight). This suggested the double-well oscillator $\ddot{x} - x + x^3$ as a starting step. To implement the symmetry breaking (detuning in the original system), the quadratic term was added, and it was natural to attach it to a variable parameter, $\beta$. Thereafter, one needed the oscillator to exhibit limit cycles, so one needed a negative damping term with a saturation value. Putting all together, the equation (10) was arrived at. The ultimate justification of (10) as a faithful representation of (6) is that they both have the features which one intends to demonstrate. The strength $b$ of the negative damping in the simplified system is analogous to the coupling $\alpha$ in the original, while the coefficient $\beta$ of the quadratic term is analogous to the detuning $k_1$.

In the absence of the asymmetry $\beta$, the equilibria of the system are -1, 0 and 1. At $b = 0$, the -1 and +1 ends are centres while the origin is a saddle. When $b$ is made positive, the centres turn into unstable foci thereby showing a Hopf bifurcation. Numerical integration of (6) yields the following features. For $\beta = 0$, at sufficiently small values of $b$, there are two stable limit cycles, one surrounding each unstable focus. At $b = 0.33$ however, the two merge into one big limit cycle which has figure-of-eight (or more appropriately "peanut") shape in the phase plane. When $\beta$ is non-zero, at sufficiently small $b$ there are two limit cycles surrounding the two unstable foci. Upon increasing $b$, the limit cycle on the right first hits the origin and disappears while the left one remains intact. Upon further increase of $b$, the peanut shaped limit cycle appears in coexistence with the left side cycle while still later the left side cycle also hits the origin and vanishes.

Melnikov's method [27] is used to analytically generate the bifurcation curves. The steps shall be shown in detail for the analysis of the limit cycle on the right side of the phase plane. For this, we first define a new variable $y = x - x*$ where $x* = -\beta + \sqrt{\beta^2 + 4}$ is the fixed point at positive $x$. Our ODE then becomes

$$\ddot{y} + C_1 y + C_2 y^2 + y^3 - b\dot{y} + \dot{y}^3 = 0 \tag{11}$$

where

$$C_1 = 2 + \frac{\beta}{2}\left(\beta - \sqrt{\beta^2 + 4}\right) \tag{12a}$$

$$C_2 = \frac{1}{2}\left(\beta - 3\sqrt{\beta^2 + 4}\right) \tag{12b}$$

The first four terms in (10) make up a conservative system, while the next two terms are the perturbation which drives a limit cycle. Following standard Melnikov procedure, we attach a coefficient of $\varepsilon$ to these terms (it is a parameter which is initially

assumed small, and can later be set to unity) and let $P$ ("momentum") denote $dy/dt$. Thus, we have the structure

$$\dot{y} = \frac{\partial H}{\partial P} + \varepsilon g_1 \tag{13a}$$

$$\dot{P} = -\frac{\partial H}{\partial y} + \varepsilon g_2 \tag{13b}$$

where $H$ is the Hamiltonian

$$H = \frac{1}{2}\dot{y}^2 + \frac{C_1}{2}y^2 + \frac{C_2}{3}y^3 + \frac{1}{4}y^4 \tag{14}$$

$g_1 = 0$ and $g_2 = b\dot{y} - \dot{y}^3$. The criterion [3] for the occurrence of the homoclinic bifurcation is that the time integral of $g_2(\partial H/\partial P)$ over one homoclinic orbit of the unperturbed system be identically zero i.e.

$$\oint \left(b\dot{y} - \dot{y}^3\right)\dot{y}\mathrm{d}t = 0 \tag{15}$$

where the integral is to be taken over one homoclinic orbit of the conservative system. This orbit is the one which passes through the saddle point $x = 0$ with zero velocity. Since $x = 0$ corresponds to $y = -x*$, the total energy of the critical orbit is

$$E_{cr} = \frac{C_1}{2}x*^2 + \frac{C_2}{3}x*^3 + \frac{1}{4}x*^4 \tag{16}$$

and the equation of the homoclinic trajectory is

$$\frac{1}{2}\left(\frac{\mathrm{d}y}{\mathrm{d}t}\right)^2 = E_{cr} - \frac{C_1}{2}y^2 - \frac{C_2}{3}y^3 - \frac{1}{4}y^4 \tag{17}$$

This can readily yield a differential equation for $y(t)$ on the trajectory – although this equation is separable and can be solved by transferring variables, the resulting integral has a cumbersome expression. Since numerical quadrature is required anyway to evaluate (11), the integral (13) was evaluated by computer also. This solution was then used to evaluate (11). For every fixed value $\beta$, (11) was computed, set equal to zero and solved for $b$ resulting in a curve in the $b$-$\beta$ plane. If one computes (11) along a trajectory which started slightly to the right of the saddle point with zero velocity, then one obtains the homoclinic bifurcation point of the limit cycle on the right. Similarly, for the homoclinic bifurcation of the left side limit cycle, one needs to evaluate (11) along a trajectory which starts slightly left of the saddle with zero velocity. Finally, for the homoclinic bifurcation of the peanut, one needs to choose a trajectory which passes the saddle with a very small but non-zero velocity. The three curves obtained thereby are shown in Fig. 10.

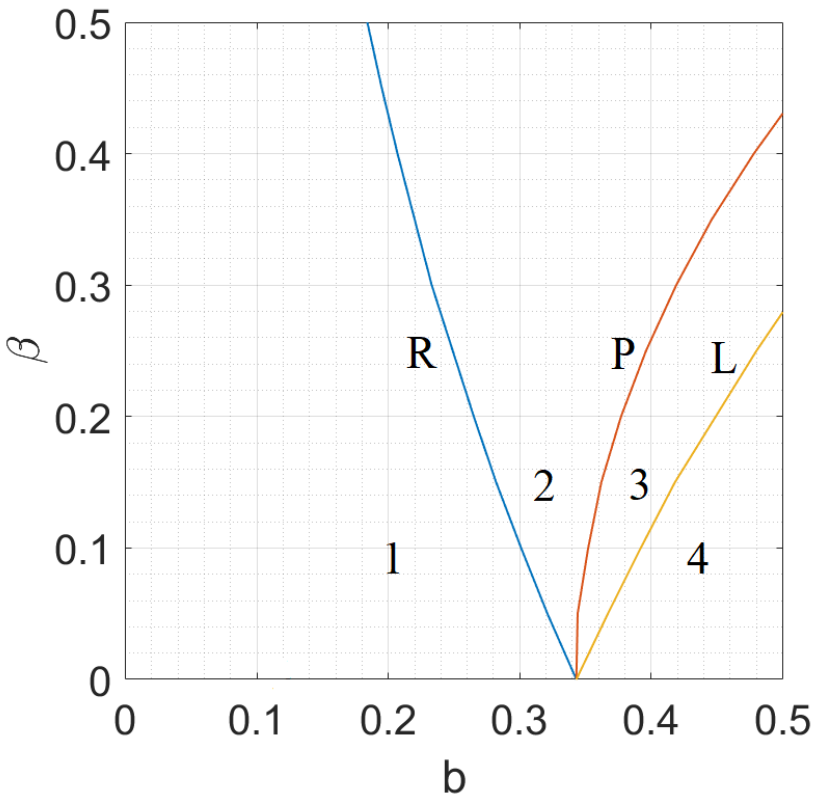


Figure 10: Melnikov's method applied to the simplified system (6). Transition curves in the $b$-$\beta$ plane for the left, right and peanut limit cycles (lines marked L, R and P respectively). These curves partition the region into four sectors, labelled 1, 2, 3 and 4. The vanishing of the integral only yields the curve without telling one on which side the limit cycle is present and absent. Numerical integration yielded that the right side limit cycle exists in region 1, the left side limit cycle exists in regions 1, 2 and 3 and the peanut exists in regions 3 and 4.

This curve shows strong similarity with the results of direct numerical integration of the system. Indeed, one can find the counter-intuitive coexistence of limit cycles which was seen in the original system also. A schematic representations of the phase portraits associated with the various regions of parameter space is shown in Fig. 11.

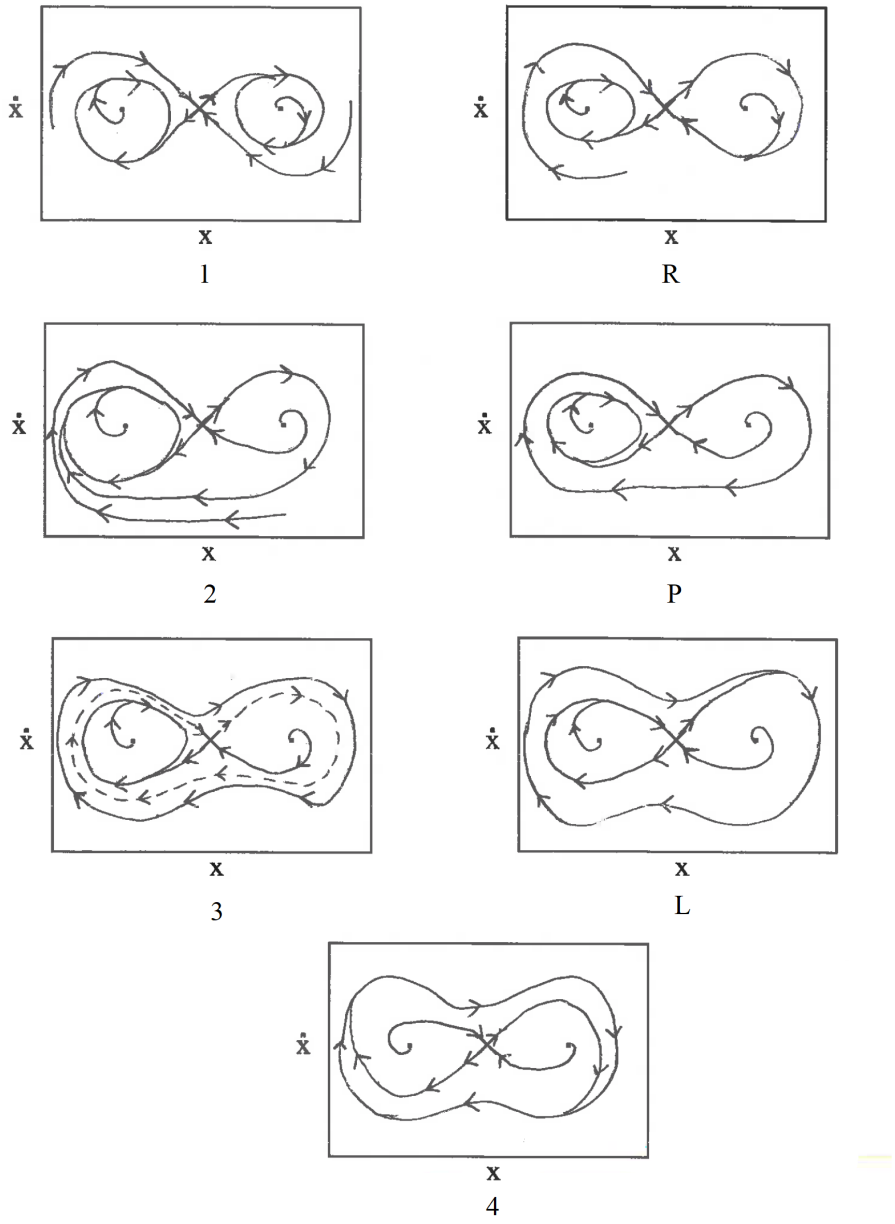


Figure 11: Schematic representation of the phase portraits of the system (6) in the various regions and transition curves shown in Fig. 10. The region/curve is labelled under each plot. Some of the portraits are self-explanatory. In "P", a coalescence [26] has occurred between the lines going forward and backward from the saddle in "2". In "3", the two stable limit cycles are separated by a homoclinic connection, which acts as the "separatrix" or boundary between the two basins of attraction.

In Fig. 12, the transition curves between the various regions are plotted numerically, using a process similar to that used for drawing Fig. 9. The similarity with the curves obtained from the Melnikov method is noteworthy.

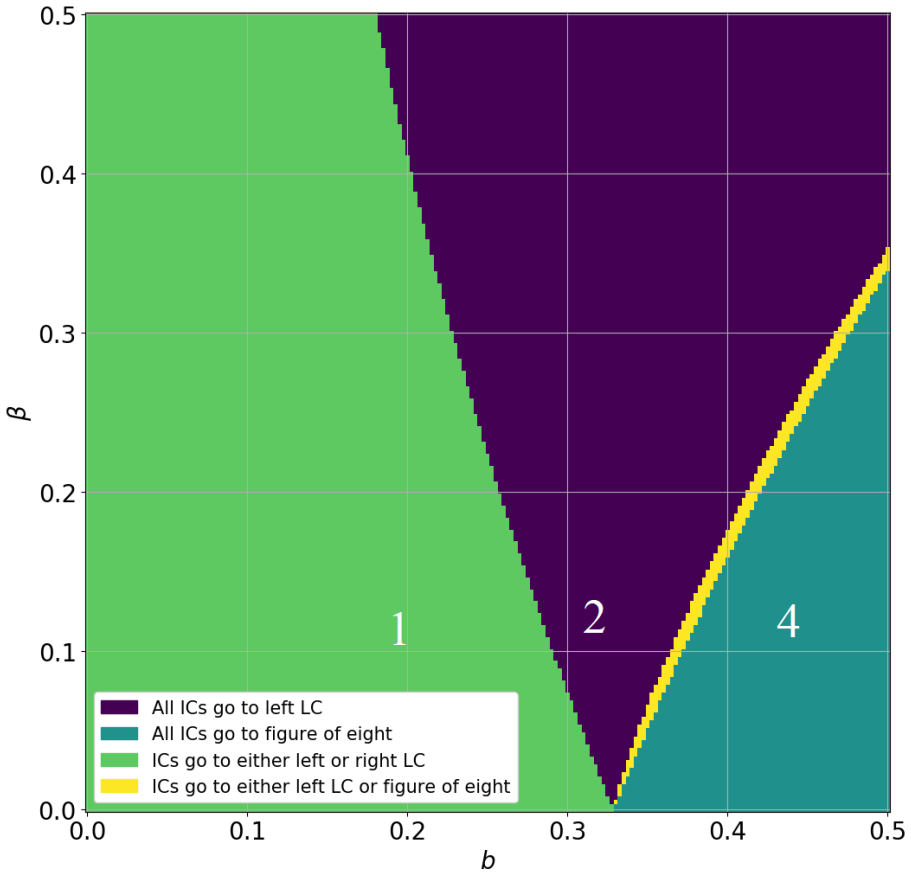


Figure 12: Simulation results for the simplified equation (6). Green indicates coexistence of the left and right side limit cycles, purple indicates left limit cycle alone, aqua denotes peanut orbit alone while yellow shows coexistence of the left side limit cycle and the peanut orbit. The similarities with Fig. 9 are apparent if one takes into account the extra complexity arising in the third order system.

A summary is now given of how the simplified system (6) relates to the original one (2). In the original system, reducing $\alpha$ causes supercritical Hopf bifurcations of the two heretofore stable equilibria. Here, increasing $b$ through zero causes the same bifurcations. Hence it can be said that $b$ is the equivalent of $\alpha$. The quadratic term $\beta$ introduces asymmetry – in the absence of asymmetry the two limit cycles are identical and undergo the homoclinic bifurcation simultaneously into a figure of eight. This is analogous to the two identical oscillators of Reference [1]. Increasing $\beta$ in the sim-

plified system is equivalent to increasing the detuning on the actual system hence we can say that $\beta$ is the equivalent of $k_1$. For a fixed $\beta$ (respectively $k_1$), increasing $b$ (decreasing $\alpha$) causes the homoclinic bifurcations, first of one limit cycle and then of the other.

The similarities between Figs. 9 (left side) and 12 may also be noted in this regard. For example, in Fig. 9 consider the fixed value $k = 0.002$ and move leftward along this horizontal line. In region E, at about $\alpha = 0.0435$ one has a small limit cycle on either side of the saddle (IP). At $\alpha = 0.0429$ approximately, the large limit cycle (figure-of-eight) is born and coexists with the small cycle. At $\alpha = 0.0425$, the small limit cycle disappears. Similarly in Fig. 12, consider the fixed value $\beta = 0.1$ and move rightwards along the graph. At $\alpha = 0.32$ approximately, one has one small limit cycle; the peanut appears at about 0.36 coexisting with the small cycle while the latter disappears at about $\alpha = 0.37$.

# 5 Summary of bifurcations, conclusion

The dynamics of two MEMS-inspired detuned oscillators has been considered in this work. A very rich bifurcation sequence is observed, with the symmetry of the structures being broken by the detuning. This bifurcation sequence is shown in a schematic form in Fig. 13. A new schematic representation is employed here, which was invented by the authors in a recent work [29]. Each diagram only enumerates the various objects present without attempting to describe their location. Fixed points are shown as dots and limit cycles as ellipses. The special figure-of-eight limit cycle is shown as an '8'. Any object which is stable is surrounded by a red box whereas an unstable object does not have this box.

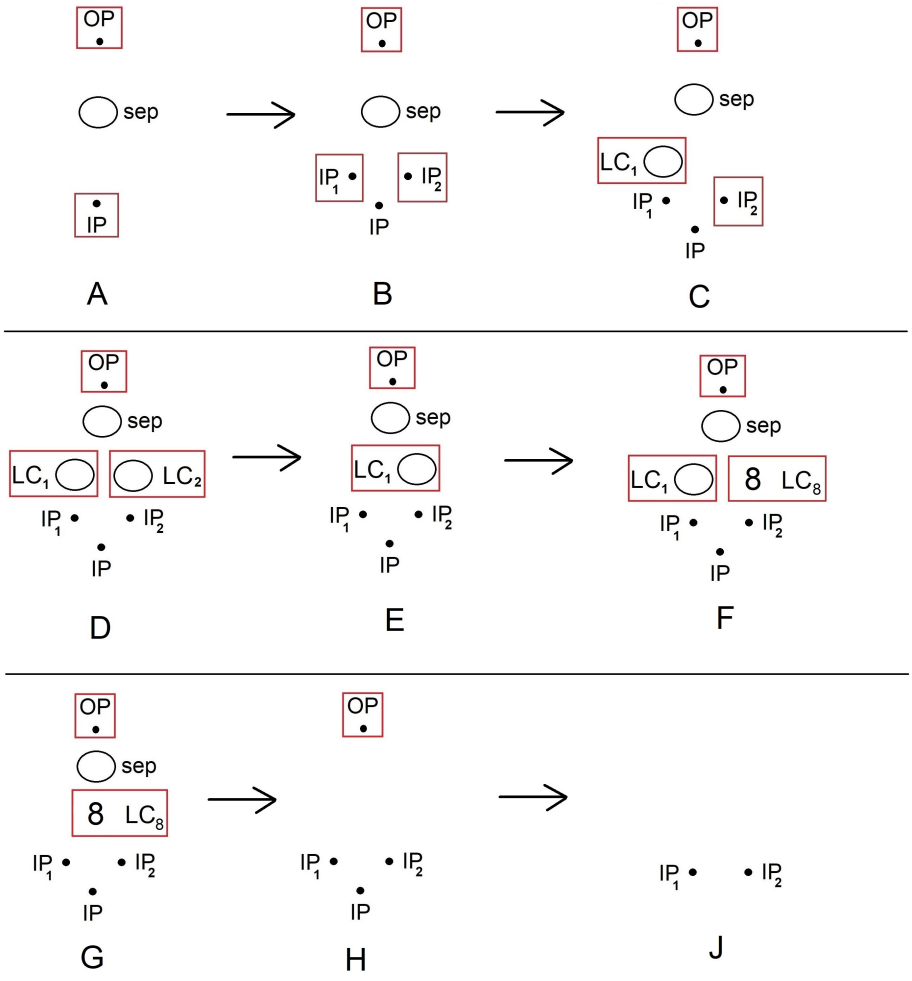


Figure 13: Schematic representation of the sequence of bifurcations occurring in the slow flow (5) as the coupling $\alpha$ is reduced from a high value (about 0.06) to a low value (close to zero). The detuning $k_1$ is taken to be constant at about 0.002. After reading one line left to right, reader to proceed to the next line. It is noteworthy how the initially simple structure becomes more complicated before again returning to a simple structure. Note also that the figure-of-eight limit cycle is denoted by LC8 and indicated by an '8'. 'Sep' denotes the separatrix between the IP and OP modes.

A summary list of the bifurcations taking place in the above Figure is given below:

- Region A is high $\alpha$ where there are only the stable IP and OP modes and an unstable limit cycle (separatrix) separating the two.
- A saddle-node bifurcation occurs from A to B giving rise to a new pair of stable

fixed points, while destroying the stability of the IP mode.

- From B to C, IP1 loses stability in a Hopf bifurcation.
- From C to D, IP2 loses stability in a Hopf bifurcation.
- The first of the homoclinic bifurcations occurs from D to E - LC2 collides with the saddle-like IP mode and vanishes.
- The most interesting bifurcation of this Article occurs from E to F - a trajectory emanating from IP2 collies in a homoclinic bifurcation with a trajectory approaching LC1, giving rise to the stable LC8 which coexists with LC1.
- A third homoclinic bifurcation occurs from F to G - LC1 collides with IP and vanishes.
- From G to H, a saddle node bifurcation of cycles causes LC8 to collide with the separatrix.
- From H to J, a saddle node bifurcation causes IP and OP modes to coalesce. From this point onwards, the two oscillators drift with respect to each other.

In conclusion, a simplified second order model of the system has also been constructed, and its analysis has yielded important information regarding the bifurcation structure in the original system. Specifically, it has been found that a peanut or figure-of-eight shaped limit cycle is born in a homoclinic bifurcation off the approach path to a more conventionally shaped limit cycle, and this leads to coexistence of the circular and figure-of-eight limit cycles in some region of the parameter space.

The various kinds of coexisting motions at the same point in parameter space have important practical consequences. For example, one may want a situation where one can switch between IP and OP modes in the same system, or a situation where one can switch between small and large limit cycles. It appears that to achieve these switches in the present system, one need not adjust the parameters but only has to adjust the initial conditions with which the system is started. In subsequent works it is hoped to obtain results for many coupled oscillators, which may reasonably be expected to support multiple coexisting modes and display a very complicated sequence of bifurcations.

# 6 Acknowledgement

This material is based upon work supported by the National Science Foundation (NSF) under grant number CMMI-1634664. This work used allocation TG-MSS170032 at the Extreme Science and Engineering Discovery Environment (XSEDE), which is supported by NSF grant number ACI-1548562. Specifically, it used the Bridges system, which is supported by NSF award number ACI-1445606, at the Pittsburgh Supercomputing Center (PSC). Indebtedness is expressed to the anonymous Reviewers whose suggestions resulted in significant improvements to the quality of the manuscript. Thanks are also due to F. Lakrad for valuable discussion.

# References


[1] RH Rand, AT Zehnder, B Shayak and A Bhaskar, "Simplified model and analysis of a pair of coupled thermo-optical MEMS oscillators," Nonlinear Dyanamics, Special Issue in memoriam AH Nayfeh (2019)

[2] AT Zehnder, RH Rand and S Krylov, "Locking of electrostatically coupled thermo-optically driven MEMS limit cycle oscillators," International Journal of Non-Linear Mechanics 102, 92-100 (2018)

[3] KE Petersen, "Micromechanical membrane switches on silicon," IBM Journal of Research and Development, 23 (4), 376-385 (1979)

[4] RH Ma et. al., "A Microcantilever-based gas flow sensor for flow rate and direction detection," Microsystem Technologies 15 (8), 1201-1205 (2009)

[5] B Pratiher, "Stability analysis of an electrostatically controlled highly deformable microcantilever based resonator," Nonlinear Dynamics 78 (3), 1781-1800 (2015)

[6] S Dhakane and WV Patil, "Piezo-resistive method for tuberculosis detection using microcantilever biosensor," ibid. 20 (3), 457-462 (2014)

[7] DK Parsediya, J Singh and PK Kankar, "Variable width based stepped MEMS cantilevers for micro or pico level biosensing and effective switching," Journal of Mechanical Science and Technology 29 (11), 4823-2832 (2015)

[8] MZ Ansari and C Cho, "An Optimized silicon piezoresistive microcantilever sensor for surface stress studies," Microsystem Technologies 22 (9), 2279-2285 (2016)

[9] HJT Smith, JA Blackburn and GL Baker, "Experimental observation of intermittency in coupled chaotic pendulums," International Journal of Bifurcation and Chaos 9 (10), 1907-1916 (1999)

[10] VYT Yolong and P Woafo, "Dynamics of electrostatically actuated micro-electromechanical systems : single device and arrays of devices," ibid. 19 (3), 1007-1022 (2009)

[11] TG Amorim, WG Dantas and A Gusso, "Analysis of the chaotic regime of MEMS/NEMS fixed-fixed beam oscillators using improved 1-DOF model," Nonlinear Dynamics 79 (2), 967-981 (2015)

[12] IT Georgiou and F Romeo, "Multi-physics dynamics of a mechanical oscillator coupled to an electromagnetic circuit," International Journal of Nonlinear Mechanics 70 (1), 153-164 (2015)

[13] V Settini and F Romeo, "Dynamic regimes of a nonlinearly coupled electromagnetic system," ibid. 103 (1), 68-81 (2018)

[14] O Shoshani, MI Dykman and SW Shaw, "Tuning linear and nonlinear characteristics of a resonator via nonlinear coupling with a secondary resonator," in press, Nonlinear Dynamics (2019)

[15] K Aubin, M Zalalutdinov, T Alans, RB Reichenbach, RH Rand, AT Zehnder, J Parpia and HG Craighead, "Limit cycle oscillations in CW laser-driven NEMS," Journal of microelectromechanical systems 13 (6), 1018-1026 (2004)

[16] S Leadenham and A Erturk, "Unified electroelastic dynamics of a bimorph piezoelectric cantilever for energy harvesting, sensing and actuation," Nonlinear Dynamics 79 (3), 1727-1743 (2015)

[17] S Leadenham and A Erturk, "Mechanically and electrically nonlinear non-ideal piezoelectric energy harvesting framework with experimental validations," ibid. volume pending (2019)

[18] A Garg and SK Dwivedi, "Nonlinear dynamics of parametrically excited piezoelectric energy harvester with 1:3 internal resonance," International Journal of Nonlinear Mechanics 111 (1), 82-94 (2019)

[19] AP Kuznetsov, SP Kuznetsov and NV Stankevich, "A Simple autonomous quasiperiodic self-oscillator," Communications in Nonlinear Science and Numerical Simulation 15 (6), 1676-1681 (2010)

[20] AP Kuznetsov, SP Kuznetsov, E Mosekilde and NV Stankevich, "Coexisting hidden attractors in a radio-physical oscillator system," Journal of Physics A 48 (12), 125101 (2015)

[21] R Krishnan, "Electric Motor Drives - Modeling, Analysis and Control," PHI Learning Private Limited, New Delhi (2010)

[22] J Holtz, "On the spatial propagation of transient magnetic fields in ac machines," IEEE Transactions on Industry Applications 32 (4), 927-937 (1996)

[23] GA Leonov et. al., "Hidden oscillations in mathematical model of drilling system actuated by induction motor with a wound rotor," Nonlinear Dynamics 77 (1), 277-288 (2014)

[24] C Tunc and M Ates, "Stability and boundedness results for solutions of certain third order nonlinear vector differential equations," Nonlinear Dynamics 45 (3), 273-281 (2006)

[25] EJ Doedel et. al., "AUTO 07p : Continuation and bifurcation software for ordinary differential equations," (2008)

[26] JW Hubbard and BH West, "Differential Equations : a Dynamical Systems Version," Spriner Verlag, Heidelberg, Germany (1995)

[27] RH Rand, "Lecture Notes on Nonlinear Vibrations," 54th edition, Published on-line by The Internet-First University Press (2012). Available electronically at http://ecommons.library.cornell.edu/handle/1813/28989

[28] CM Bender and SA Orszag, "Advanced Mathematical Methods for Scientists and Engineers," Springer Verlag, Heidelberg, Germany (1988)

[29] RH Rand, AT Zehnder, B Shayak and A Bhaskar, "Dynamics of a system of two coupled MEMS oscillators," Chapter 20 of IUTAM Symposium on Exploiting Nonlinear Dynamics in Engineering Systems, Springer Verlag, Berlin, Germany (2019)

# 7 Appendix

The WXMaxima code used for obtaining analytical formula for the saddle node bifurcation curves is given below.

```
kill(all);

eqs:['diff(r1,zeta,1) = (-(alpha*sin(phi)*r2)/2)-(9*r1^3)/40+(p*r1)/4,
'diff(r2,zeta,1) = (-(9*r2^3)/40)+(p*r2)/4+(alpha*sin(phi)*r1)/2,
'diff(phi,zeta,1) = (31*r2^2)/120-(alpha*cos(phi)*r2)/(2*r1)
+(alpha*cos(phi)*r1)/(2*r2)-(31*r1^2)/120
-k1/2];
p:1/10;
foo1:solve(part(eqs,1,2),sin(phi));
foo2:solve(part(eqs,2,2),sin(phi));
foo3:solve(part(eqs,3,2),cos(phi));
foo4:sin(phi)^2+cos(phi)^2-1,foo1,foo3;
foo5:sin(phi)^2+cos(phi)^2-1,foo2,foo3;

foo6:num(ratsimp(foo4));
foo7:num(ratsimp(foo5));

foo8:eliminate([foo6,foo7],[r2]);
foo9:factor(%);
foo10:first(last(last(foo9)));
foo11:foo10,k1=0;
foo12:factor(%);

foo13:diff(foo10,r1);
/* double root */
eliminate([foo10,foo13],[r1]);
factor(%);
goo1:part(%,1);
goo2:part(%,6,1);
/* choose power of k1 s.t. there is a distinguished limit */
goo2,alpha=31/540+k1^(2/3)*beta;
expand(%);
coeff(%,k1,2);
solve(%,beta);
alpha=31/540+k1^(2/3)*beta,last(%);
```

```
%,k1=.002,numer;
/* fold corresponding to pitchfork at k1=0 */

dummy;
```